# EPICS, the exoplanet imager for the E-ELT

Markus E. Kasper[1a], Jean-Luc Beuzit[b], Christophe Verinaud[b], Natalia Yaitskova[a], Pierre Baudoz[c], Anthony Boccaletti[c], Raffaele G. Gratton[d], Norbert Hubin[a], Florian Kerber[a], Ronald Roelfsema[e,j], Hans Martin Schmid[f], Niranjan A. Thatte[g], K. Dohlen[h], M. Feldt[i], Lars Venema[e], S. Wolf[k]

[a]European Southern Observatory, Karl-Schwarzschild-Str. 2, D-85748 Garching, Germany
[b]LAOG, 414 Rue de la Piscine, 38400 Saint-Martin d'Hères, France
[c]LESIA, Observatoire de Paris-Meudon, 5 place Jules Janssen, 92195 Meudon Cedex, France
[d]Osservatorio Astronomico di Padova, Vicolo dell'Osservatorio 5, 35122 Padova, Italy
[e]ASTRON, Oude Hoogeveensedijk 4, 7991 PD Dwingeloo, The Netherlands
[f]ETH Zürich, Institute of Astronomy, HIT, CH-8093 Zürich, Switzerland
[g]University of Oxford, Wellington Square, Oxford OX1 2JD, United Kingdom
[h]LAM, 38 Rue Frédéric Joliot-Curie, 13388 Marseille Cedex 13, France
[i]Max-Planck-Institut für Astronomie, Königstuhl 17, 69117 Heidelberg, Germany
[j]NOVA, Universiteit Utrecht, P.O. Box 80000, NL-3508 TA Utrecht, The Netherlands
[k]Christian-Albrechts-Universität zu Kiel, Leibnizstr. 15, 24098 Kiel, Germany

## ABSTRACT

Presently, dedicated instrument developments at large telescopes (SPHERE for the VLT, GPI for Gemini) are about to discover and explore self-luminous giant planets by direct imaging and spectroscopy. The next generation of 30m-40m ground-based telescopes, the Extremely Large Telescopes (ELTs), have the potential to dramatically enlarge the discovery space towards older giant planets seen in reflected light and ultimately even a small number of rocky planets. EPICS is a proposed instrument for the European ELT, dedicated to the detection and characterization of expolanets by direct imaging and spectroscopy. ESO recently launched a phase-A study for EPICS with a large European consortium which - by simulations and demonstration experiments - will investigate state-of-the-art diffraction and speckle suppression techniques to deliver highest contrasts. The final result of the study in 2010 will be a conceptual design and a development plan for the instrument. Here we present first results from the phase-A study and discuss the main challenges and science capabilities of EPICS.

**Keywords:** XAO, ELT, high contrast imaging, extrasolar planets, instrumentation, adaptive optics

## 1. INTRODUCTION

### 1.1 The EPICS phase-A study for the E-ELT

The Exo-Planet Imaging Camera and Spectrograph (EPICS) is an instrument project for the direct imaging and characterization of extra-solar planets with the European ELT (E-ELT). EPICS will be optimized for observations in the visible and the near-IR and will have photometric, spectroscopic and polarimetric capabilities.

The E-ELT is currently going through a phase-B study which will include an instrumentation plan with the list of first generation instruments. The highest priority scientific objectives (which include Exoplanets) will dictate the choice of the first generation instruments. The EPICS phase-A study is one of these E-ELT instrument studies and has been kicked off in October 2007. Among the goals of EPICS phase-A study, requirements to the telescope and the associated site should be clearly addressed and feedback should be provided to the E-ELT Design Reference Missions. The final study report will include the calculated scientific capabilities, cost, FTE effort and a construction schedule. It will be the basis for the technical specifications and statement of work of the construction contract, should the priority and feasibility of EPICS be confirmed.

[1] mkasper@eso.org; phone 49 89 3200 6359; www.eso.org

The EPICS phase-A study is carried out by a large European consortium led by ESO and LAOG as PI and Co-PI institutes (see Figure 1), and is partially funded by ESO and the European Framework Programme 7 (FP7).

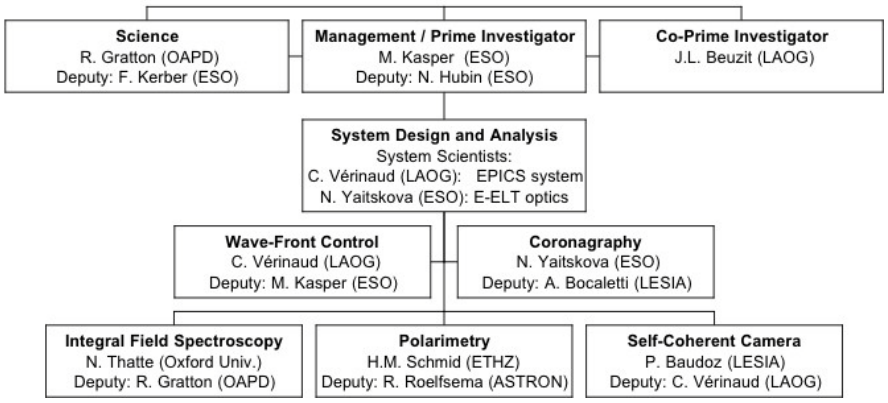


**Figure 1. EPICS consortium organization and workpackages.**

### 1.2 Science Motivation

EPICS will be optimized, and trade-offs made, focusing on the following prominent exoplanet science cases:

1. Detection of young self-luminous gas giants in star forming regions or young associations with the goal to determine initial frequency and mass distribution of giant planets and to study planet formation.
2. Detection and characterization of mature gas giants at orbital distances between ~5 and 15 AU in the solar neighborhood (< ~20 pc) with the goal to determine frequency and mass distribution of giant planets not easily accessible to radial velocity, astrometric or photometric techniques.
3. Imaging and spectral characterization of warm or young Jupiters that have been previously discovered by radial velocity searches or direct imaging with smaller telescopes with the goal is to understand giant planets' atmospheric composition and structure. Some tens of currently known targets are readily observable with EPICS as shown in Figure 2, and many more may be known from upcoming observations with e.g. GAIA or SPHERE.
4. Detection and 1st order characterization of Neptune mass planets and massive rocky planets around nearby stars (≤ 10 pc) with the ultimate goal of detecting such planets located in the habitable zone (for late type stars and very nearby systems ≤ 4 pc).

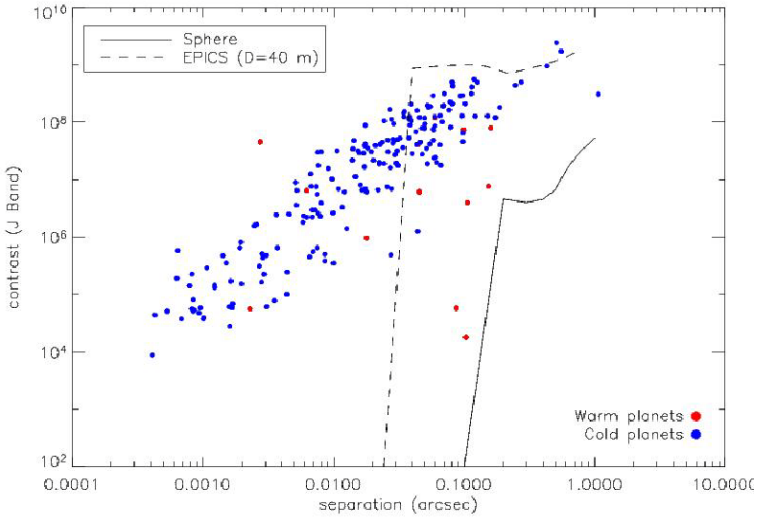


**Figure 2. Contrast and angular resolution required to observe exoplanets known from radial velocity surveys.**

In addition, EPICS is expected to prove very useful for additional science, like tracing the surface structure in young disks. Figure 3 shows observations of AB Aurigae, where a spiral structure that could be attributed to the presence of a

planetary object within the disk is visible as the model of scattered light expected in the K-band shown on the right suggests. EPICS will be able to obtain images of the spatial dust distribution in planetary systems analogous to our own. If observed from afar, the Kuiper Belt dust disk would be the brightest spatially extended feature in the solar system. Its spatially resolved structure could be recognized as harboring at least two giant planets: an inner planet (Jupiter/Saturn) and an outer planet (Neptune; Liou et al. 1999, Moro-Martin & Malhotra 2002). Thus, high-resolution, high-sensitivity imaging of debris disks around other stars will provide insights into the frequency and diversity of planetary systems, helping us to place our solar system - in particular its planets - into context.

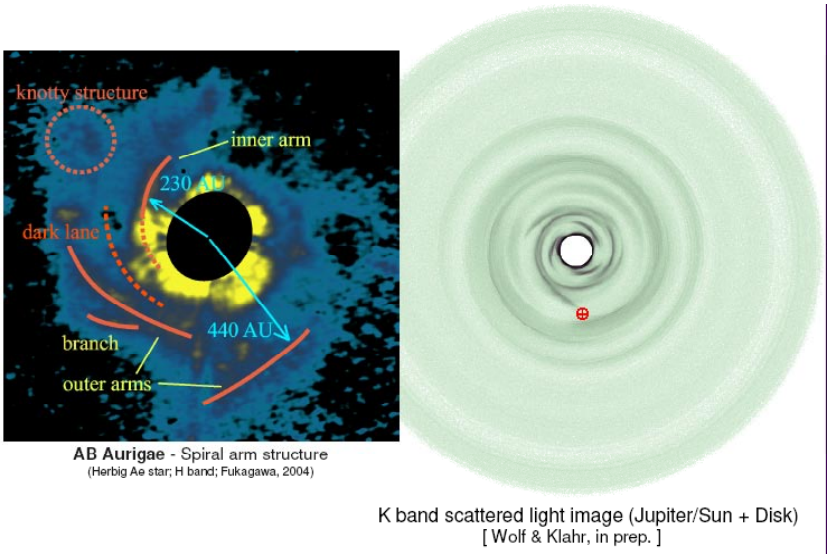


**Figure 3. Left panel: observations of the structure of the disk around the young star AB Aurigae. Right panel: Model of scattered light in the K-band for a disk including a Jupiter-size object. Dynamical perturbation by the planet cause spiral structures in the disk.**

### 1.3 Top Level requirements

The contrast Top Level Requirements in the Y-H band that are derived from these science cases are given in Table 1. For science cases 2 and 4, the contrast requirements extend to visible wavelengths for the differential polarimeter.

**Table 1. Contrast requirements in the Y-H band (10h observation, 0.7 arcsec I-band seeing, $\tau_0$=3 ms, 5σ detection, bright star)**

| Brightness ratio at distance: [mas] | 30 | 100 | 300 | Limiting AO stellar magnitude I band: |
|---|---|---|---|---|
| Science Case 1 | $10^{-6}$ | $10^{-6}$ | $10^{-6}$ | **9 (goal: 10)** |
| Science Case 2 | | **$2\ 10^{-9}$ (goal $10^{-9}$)** | **$10^{-9}$ (goal $4\ 10^{-10}$)** | 7 (goal: 8) |
| Science Case 3 | **$10^{-8}$** | **$10^{-9}$** | $10^{-8}$ | 7 (goal: 8) |
| Science Case 4 | $2\ 10^{-9}$ (goal $10^{-9}$) | $10^{-9}$ (goal $4\ 10^{-10}$) | $5\ 10^{-10}$ (goal $2\ 10^{-10}$) | 5 (goal: 6) |

Assuming that these contrast requirements will be achieved and considering the photon noise limit for the assumed 10h of integration time, the number of expected planet detections with EPICS as a function of mass for a sample of about 600 stars within 20 pc has been calculated and is shown in Figure 4. These estimates are based on Monte Carlo simulations, where orbital and mass distributions of planets were derived from Mordasini et al.[10]. The diagram on the left shows one realization of these Monte Carlo simulation where open circles are detected planets, filled circles when detected inside the habitable zone, and dots are planets that were not detected. Although having a contrast higher than the goal TLRs, many planets are not detected because they are too faint and hidden by photon noise rather than PSF residuals.

The histogram on the right shows the average of 100 Monte Carlo realization and predicts the detection of several hundred exo-planets, including over a dozen super-Earths (2-5 $M_{Earth}$), with a ~50% chance that at least one of them is in the habitable zone. As a sanity check, the predicted detection of around 70 giant planets with masses larger than 1 $M_{Jupiter}$

for our sample of 600 stars is consistent with the about 10% exoplanet detection rates derived from radial velocity search programs[2].

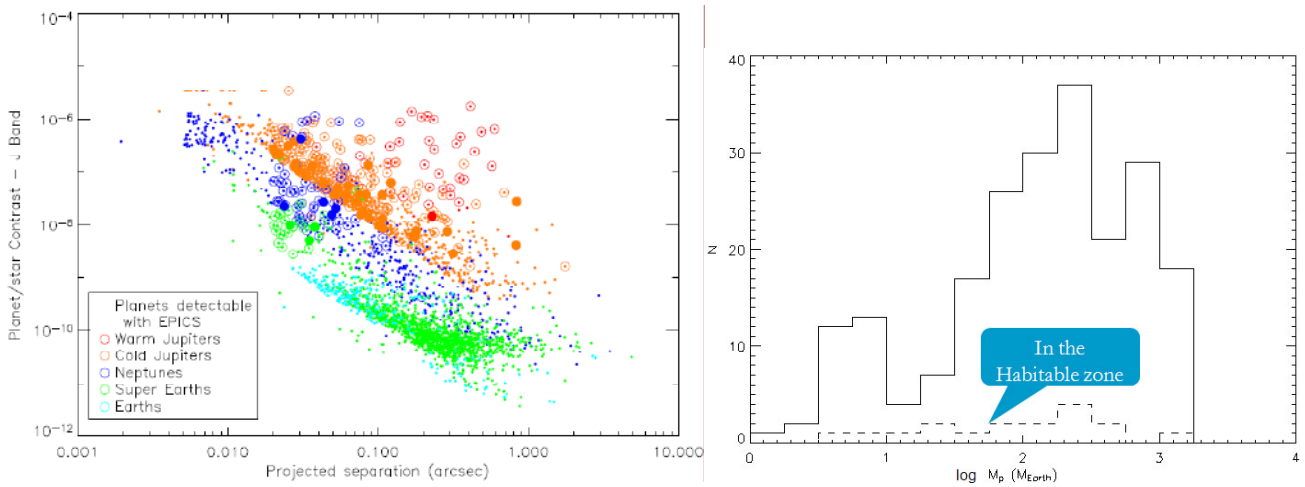


**Figure 4. Monte Carlo simulations of exoplanet detection rates with EPICS. Left: MC Realization where circles are detected planets (filled when in the HZ) and dots are missed planets. Right: Histogram of 100 averaged realizations.**

### 1.4 Preliminary concept

Figure 5 outlines the basic concept of EPICS. This concept follows the standard approach to the high-contrast imaging problem. An XAO system coupled to a focal plane WFS creates an extremely well-corrected image of the central star. The diffraction pattern is then removed by a coronagraph such that the remaining level of speckles created by uncorrected aberrations and coronagraph residuals is far below (typically $10^{-6}$) the uncorrected peak intensity. These PSF residuals are then calibrated and largely removed by data analysis techniques discriminating between speckles and potential faint companions based on their chromaticity (spectral deconvolution or spectral differential imaging), polarization properties (differential polarimetry), temporal-spatial behavior (angular differential imaging), or their coherence with the central source (self-coherent camera). This calibration step can further reduce PSF residuals by typically a factor $10^3$, such that the ultimately desired contrast level of around $10^{-9}$ is reached on bright sources.

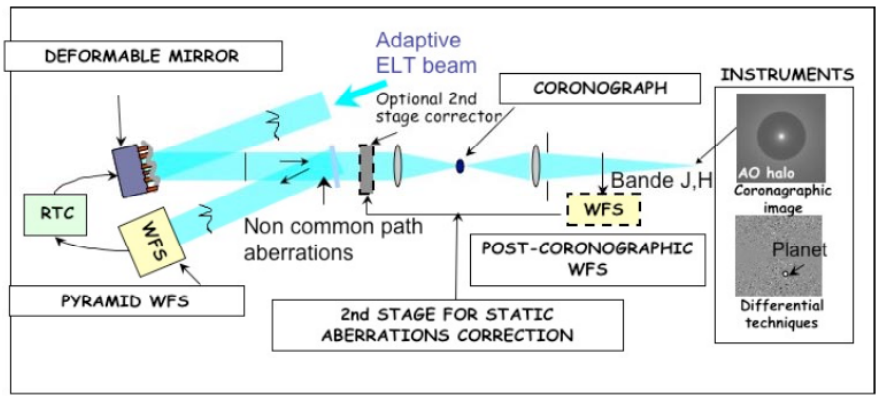


**Figure 5. Basic concept and main components of EPICS**

## 2. KEY SUBSYSTEMS AND EXPERIMENTS

### 2.1 Extreme Adaptive Optics

The XAO system is the core of EPICS. Its purpose is two-fold; firstly, it should correct for fast atmospheric aberrations and therefore efficiently reduce stellar flux and photon noise in the control region of the DM. Since the temporal

bandwidth error is dominating the AO budget, high frame-rates of about 2-3 kHz are needed to reduce the turbulent halo to the adequate level. Secondly, the XAO system must compensate for quasi-static aberrations introduced by the telescope and the instrument. A dedicated focal plane wavefront sensor (FWPS) will be implemented in EPICS to accurately measure these quasi-static aberrations.

Two kinds of wavefront sensors are considered for the EPICS XAO system, a Pyramid wavefront sensor[15] or a spatially filtered Shack-Hartmann wavefront sensor[12]. The XAO performance of these wavefront sensors has been compared by simulation[15], and a test setup (high order testbench, HOT, Aller-Carpentier et al., this conference) has been developed at ESO to investigate and compare also their practical implementation. Based on the simulations and initial HOT results (Esposito et al., this conference), the PWS has been identified as the baseline WFS of EPICS. Figure 6 shows a closed loop H-band image obtained with HOT and the PWS. In 0.5″ seeing with 3m/s wind speed, a Strehl ratio of well above 90% has been achieved running the WFS at 80 Hz framerate (limited by the RTC) and correcting for 670 modes on an 8-m pupil. This demonstrated AO performance is consistent with simulations and expected requirements for EPICS.

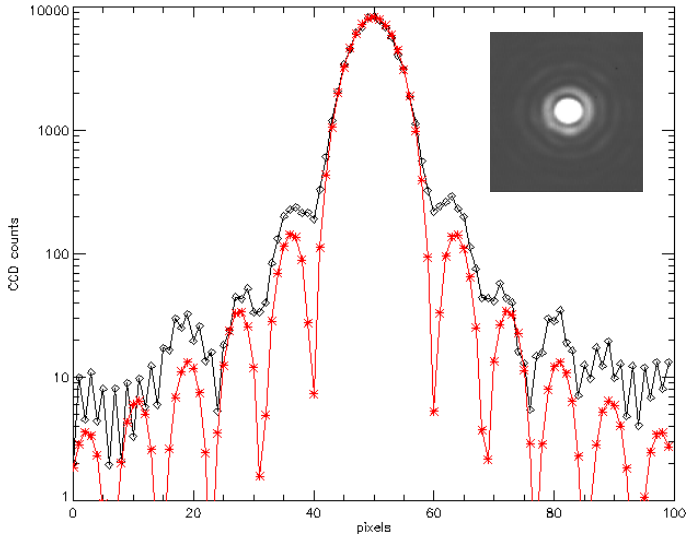


**Figure 6. HOT closed loop image obtained with the PWS in H-band (from Esposito et al., this conference).**

The EPICS XAO will have to control two deformable mirrors, the telescope M4 with about 6000 – 8000 actuators on the 42-m pupil (Vernet et al. this conference) correcting for large stroke low order aberrations and the high order DM with more than 30000 actuators (actuator spacing less than 0.2 m). A control scheme for this so-called woofer/tweeter system has been developed[4] and will be tested on HOT with its two available deformable mirrors (60 element bimorph DM and 32x32 actuators MEMS DM). In addition, HOT will be also used to evaluate the capability of the XAO system to correct for phasing errors originating from the segmented aperture of the E-ELT.

RTC computing power requirements for EPICS will be extremely challenging. Adopting the basic matrix-vector-multiplication reconstruction algorithm, the EPICS RTC would need about 1000x the computing power of the non-trivial SPHERE RTC. To overcome this problem, ESO is currently studying recent developments in CPU architecture in the frame of the E-ELT phase-B study with the goal to indentify the most promising technology. Advanced algorithm with goal to reduce required computing power are studied in the frame of the FP6 ELT design study, and this investigation will be pursued by ESO over the next years.

### 2.2 Focal Plane Wavefront Sensor

Quasi-static aberrations have a dramatic impact on the detection performance for the most demanding science objectives of EPICS. The contribution of these systematic errors will have to be lower than the coronagraphic PSF halo dominated by atmospheric turbulence residual aberrations. Hence, these systematic aberrations must be precisely measured at the (or close to the) scientific wavelength in order to minimize chromatic effects.

A dedicated focal plane wavefront sensor will measure optical aberrations at the XAO focus and scientific wavelengths and feed back the required correction to either the XAO system or to a dedicated 2$^{nd}$ stage corrector located after the

XAO. The main reason why such a 2nd stage corrector may be required is the dynamic range of the WFS limiting the wavefront error that can be offloaded to the XAO.

In the frame of the EPICS phase-A study, a novel post-coronagraphic wave-front sensor (Verinaud et al, this conference) will be developed and tested. This post-coronagraphic pupil plane ($P^3$) wavefront sensor measures wavefront phase and amplitude in a PWS similar fashion and features a very low sensitivity with respect to post-coronagraph optical aberrations.

### 2.3 Coronagraphy

A coronagraph will be located at the XAO focus and suppress the stellar diffracted light to appropriate levels of typically better than $10^{-6}$. The current baseline is to use an apodized Lyot coronagraph, but it is very likely that the final instrument will provide the flexibility to use different kinds of coronagraphs tailored to specific applications such as providing a very small inner working angle.

Various kinds of coronagraphs (Lyot, APLC, 4-QPM) have already been studied in the frame of the FP6, ELT design study, and results are presented by Martinez et al. (this conference). These studies are pursued in the frame of the EPICS phase-A study and will involve the multi-stage versions of APLC and 4-QPM as well as the dual-zone Roddier and possibly band-limited and AGPM coronagraphs. Figure 7 shows laboratory measurements of the APLC on a dedicated setup at ESO. The picture on the left shows the profile of the binary mask apodizer that nicely fulfills the profile specifications and is achromatic at NIR wavelengths. The measured coronagraphic PSF profile on the right of Figure 7, falls to about $5\times10^{-6}$ at $5\lambda/D$ (40 mas for a 42-m aperture) which will not be far from EPICS requirements.

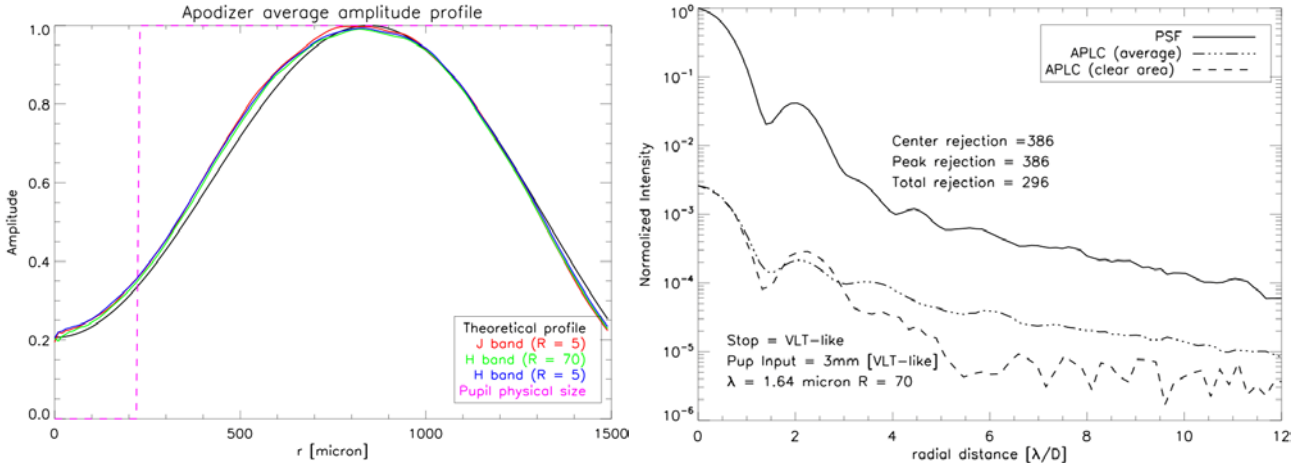


**Figure 7. Laboratory measurements of the APLC. Left: Measured profile of the binary apodizer mask, Right: Coronagraphic PSF profile. The azimuthally averaged rejection suffers from a mismatch between telescope spider arms and the Lyot stop.**

### 2.4 Integral Field Spectrograph

The coronagraphic image will be fed into two different instruments, an NIR IFS and an optical differential polarimeter. There are potentially two different designs for the IFS, lenslet based or slicer based. While the lenslet based design is basically insensitive to instrumental aberration behind the lenslet array, the slicer concept allows for a more dense arrangement of the spectra on the detector and therefore a more efficient use of the available NIR detector pixels. One option under investigation is to use a lenslet array IFS for the inner FoV and a slicer based IFS with somewhat reduced contrast requirements for the outer FoV.

In order to ensure its capability to subtract a large fraction of the residual speckles using different data reduction techniques[8,13], the following main challenges for the IFS design will be carefully analyzed during the EPICS Phase-A:

- proper sampling of the speckles in the spectral and spatial domain[1]
- impact of differential aberrations between images obtained at different wavelengths
- fidelity of the produced images (low cross talk, small flat field errors, accurate interpolation routines).

Achieving the correct sampling over the whole Field of View of EPICS (up to 2 arcsec from field center) with one lenslet-based IFS will be expensive, because of the large amount of required detector real-estate. Typically, a spacing of at least 4 detector pixels between each speclet is needed in order to achieve the cross-talk requirements. Apodization in an intermediate pupil plane can reduce the impact of cross talk between adjacent spectra and mitigate this problem. A dedicated experiment with such an apodization will be carried out at INAF-OAPD in the frame of the EPICS phase-A study.

Image slicers are possibly less demanding in terms of detector pixels, but their liability to instrumental aberrations is less clear. While the lenslet-based IFS divides the field into the individual pixels and treats them separately, the image-slicer maintains coherence in the dimension perpendicular to the slicer. Hence, the impact of instrumental aberrations on the creation of differential chromatic speckles is somewhat unclear and will be investigated by modeling and experiment during the EPICS phase-A. A suitable slicer prototype will be developed at Oxford University, the design is displayed on the right panel of Figure 8.

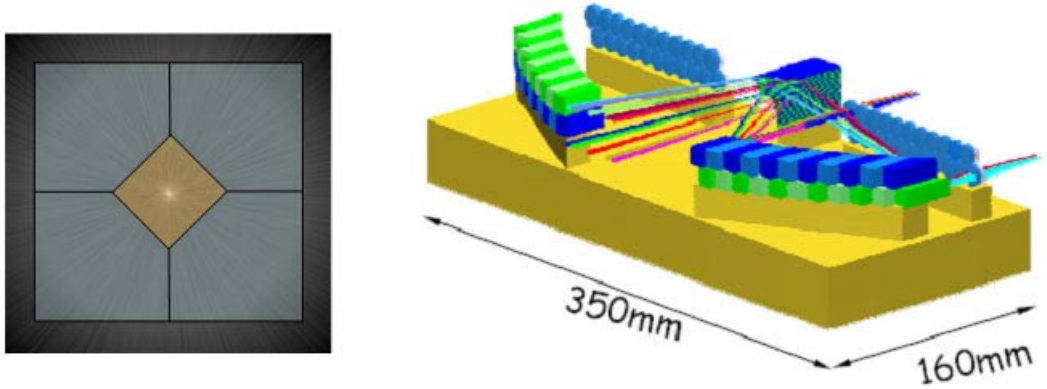


**Figure 8 Left: Possible split of the EPICS lenslet-based IFS field of view superimposed to a simulated monochromatic image. The central orange square area (0.6 arcsec side) is the most important area for exopolanet science and optimally sampled in the spatial and spectral domain. Each of the 5 IFS's requires a 4x4 k detector. Right: 3-D design of the Image Slicer prototype.**

### 2.5 Differential Polarimetry

Reflected light from planets is often very highly polarized (p > 20%) in the visual – red spectral range[16]. Since residual speckles from the central star are not polarized, differential polarimetry offers an attractive way to discriminate them from a faint companion. Rayleigh scattering by molecules and atoms or small aerosol particles are believed to be the most important processes for producing a high planet polarization. The polarization yields the optical depths of these scattering layers and the measured polarization direction tells us whether there exist strong asymmetries in the scattering geometry due to strongly polarized regions similar to the poles of Jupiter. The polarization in spectral features can be used to determine the relative abundance of scattering and absorbing particles, e.g. $H_2$ and $CH_4$ in the upper atmosphere.

Polarimetry of reflected light from extra-solar planets favors planets with small orbital separations, because the contrast between planet and star increases proportional to distance squared. Further we expect the highest polarization signal in the blue-visual spectral range due to Rayleigh scattering efficiency[17]. Hence, the polarimetric mode of EPICS (E-POL) requires small angular separations and short wavelengths. With the different wavelength regime and detection algorithm, E-POL nicely complements the NIR-IFS and provides an independent measurement dramatically reducing false alarm possibilities. A set of dichroic beamsplitters will allow for various observing modes with various options to split the light between the optical polarimeter and the WFS.

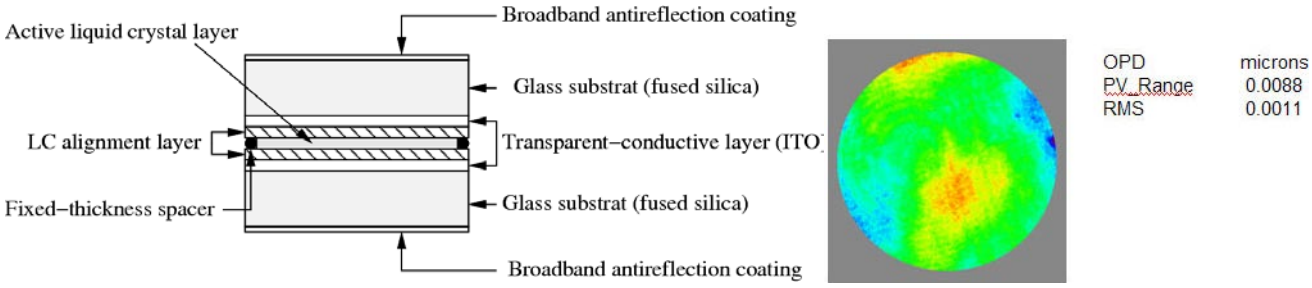


**Figure 9. Left: Cross section of an FLC modulator from BNS. Right: Measured differential wave front error of 1.1 nm after removal of tip-tilt.**

The basic principle of high precision polarization measurements includes a fast (~kHz) polarization modulator and polarizing beam-splitter to convert polarization into intensity modulation and a subsequent imaging polarimeter to demodulate the created intensity signal synchronous to the polarization modulation[16]. The final result of this concept is an almost fully differential measurement with the following key advantages:

- images for the two opposite polarization modes are created practically simultaneously if the modulation is faster than the seeing variations,
- both images are recorded with the same detector elements (same pixels) and flat-fielding problems are strongly minimized
- Differential aberrations between the two images (opposite polarization modes) can only be introduced by the polarization modulator or birefringent components in front of it; no differential aberrations are introduced by components after the modulator
- the differential (polarization) signal is not affected by chromatic effects due to telescope diffraction or speckle chromatism.

Telescope polarization in the E-ELT intermediate focus, after mirror M2, is expected to be very small (0.1% or less). Hence, it would be of great advantage to put the fast polarization modulator in the location. The modulator would convert the polarization information into intensity modulations for the two opposite linear polarization directions (say +Q and –Q) and it is quite easy to avoid strong cross talks between +Q and –Q in the instrument. The differential polarization signal which is encoded and all downstream components would introduce no differential aberrations. A very high polarimetric performance may be achievable with this approach, which is not affected by any kind of polarizing components. The calibration and data reduction for such an instrument would be very simple.

However, key requisites of this approach are that i) the polarization modulator does not introduce differential aberrations and ii) the AO WFS is not disturbed by the fast polarization modulator. Current state-of-the-art ferro-electric liquid crystal (FLC) polarization modulators (see Figure 9, left) introduce about 1 nm rms of WFE (see Figure 9, right). In the framework of the EPICS Phase-A study it is planned to procure FLCs with even lower differential aberrations and study their impact on XAO performance with HOT.

## 3. PRELIMINARY ANALYSIS

During the first part of the EPICS phase-A study, a thorough end-to-end model of EPICS from atmospheric disturbance to the reduced science image will be created and allow for detailed trade-off studies and determination of the important system parameters. These studies are still on-going, so just some preliminary analysis and considerations to better understand the problem and to constrain the main specifications of EPICS will be provided in this section.

### 3.1 Data analysis, speckle calibration

The baseline data reduction techniques for the IFS is spectral deconvolution (SD[13,14]). This technique relies on the smooth scaling of the position of almost all stellar PSF features (Airy pattern, speckles, etc.) with wavelength, whereas a physical object's location is independent of wavelength. Thus, stepping through the wavelength axis of an IFS data cube at a fixed spatial location (e.g. the location of a companion), one would see a modulation arising from the PSF features passing through the companion's location. For SD instead, the data cube is re-scaled in the spatial domain inversely proportional to the wavelength such that the position of PSF features is fixed and the companion’s position varies with

wavelength. The companion's light now traces a diagonal line through the data cube producing a “bump” in the smoothly varying spectra of an individual pixel.

Fitting a low-order polynomial to every pixel of the data cube, one obtains a very high-S/N estimate of the PSF residuals at each wavelength of the data cube. Since the low-order polynomial will not be able to fit the companion’s high frequency modulation, the light from the parent star can be subtracted from each scaled slice of the data cube, and the result scaled back to the original grid, forms a very high contrast image of the companion.

The chromatic elongation of PSF residuals is proportional to their radial distance from the center. Once this elongation is comparable to the angular size of the companion at small radial distance from the PSF center, SD would begin to subtract out also the companion’s light and to decrease the method’s efficiency. Hence there is a minimum angular separation (bifurcation point[14]) for SD which depends on the IFS spectral bandwidth. For the EPICS IFS with a wavelength coverage of about 1 – 1.7 μm, the bifurcation point would be at around 30 mas. At even shorter separations (if permitted by the coronagraph inner working angle), other data reduction techniques such as multi-wavelength spectral differential imaging would be more efficient.

The results of an initial test of the SD method are shown in Figure 10. Assuming a spectral range of ~0.95-1.735 μm at R~500–900 and various kinds of static achromatic aberrations (primary segment piston and tiptilt of 90 nm rms, segment mis-figure of 30 nm rms, 20 nm rms of high spatial frequency aberrations for each of the 5 telescope mirrors, 5 nm quasi-static calibration error of the XAO ($f^0$, flat spectrum), and 1% reflectivity dispersion) SD permits the rejection of speckles by up to a factor $10^4$. This simulation does not yet consider atmospheric turbulence residuals, Fresnel propagation of out-of-pupil aberrations and coronagraph chromaticity. It is therefore an idealized case, which will be refined at a later stage of the study.

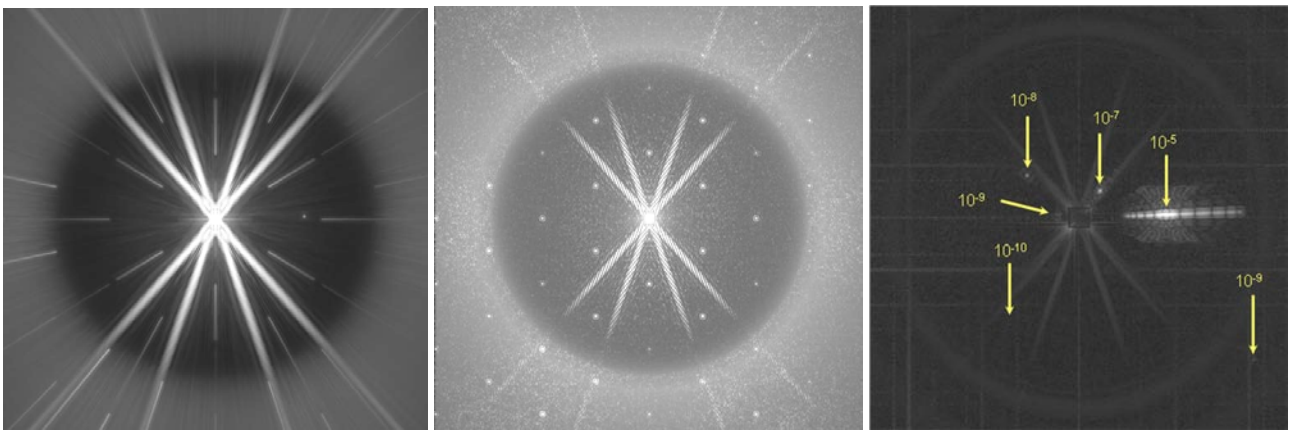


**Figure 10. IFS data reduction with static aberrations only and perfect coronagraph. Left: Wide – band image showing speckle elongation. Niddle: Spatially rescaled version of image on te left. Speckles are point-like, the hidden planets are elongated. Right: SD subtraction of residual PSF, the contrast is efficiently enhanced.**

Data reduction for the differential polarimeter will be much simpler. E-POL will produce images of identical wavelength coverage on identical detector pixels. Also there should not be any differential aberrations apart from the ≤ 1 nm rms post-coronagraphic differential aberration introduced by the FLC. Hence, the envisioned data reduction scheme is direct polarimetric differential imaging where the impact of FLC aberrations are calibrated by rotating the polarization angle with a half-wave-plate located in the XAO common path.

All observing modes of EPICS will further benefit from field rotation in the E-ELT Nasmyth focus that will rotate the companion with respect to instrumental speckles and allow for a technique called angular differential imaging (ADI[9]) where images separated by a suitable time gap (long enough to rotate the field by the angular size of the planet) are subtracted from each other removing PSF residuals while leaving the companion. The ADI gain depends on many parameters such as object position on sky, available FoV, angular separation of the companion and duration of the observation. It will be studied quantitatively at a later stage of the EPICS Phase-A. For now, we conservatively do not consider the improved speckle calibration expected from ADI.

### 3.2 Atmospheric turbulence

The lifetime of second order speckles dominating the coronagraphic residual PSF is about 0.6D/v irrespective of the behavior of the XAO system[7]. Hence, for EPICS (telescope diameter D = 42 m) and an assumed effective windspeed of v = 10m/s, the atmospheric speckle lifetime is of the order of a couple of seconds. The average intensity of these speckles for an XAO system is typically of the order of $10^{-5}$-$10^{-6}$ of the intensity of the stellar Airy peak. For a typical EPICS target star of magnitude 5, this results in a flux of about 1500 photons per speckle in the NIR for a spectral resolution R=50. Since the corresponding photon noise of sqrt(1500) is higher than the expected systematic calibration error (conservative assumption is $10^{-3}$, see section 3.1), it will dominate the atmospheric speckle residuals. In order to reduce this noise component, the atmospheric speckle intensity must be reduced. Figure 11 shows an analytical behavior of the various EPICS XAO residuals error sources. Obviously the temporal error (servo-lag) dominates at most spatial frequencies, and the only way to reduce residual atmospheric speckles is to further increase the XAO correction temporal bandwidth.

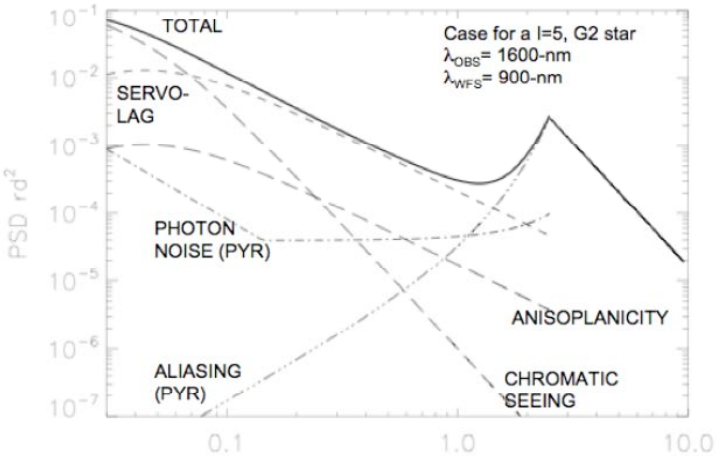


**Figure 11. Analytical profile of the turbulent coronagraphic PSF provided by the EPICS XAO concept (modulated PWS, actuator spacing 0.2-m, framerate 3kHz). Even at the high frame-rate of EPICS, the temporal error (servo-lag) is dominating the residual WFE.**

### 3.3 Quasi-static PSF residuals

The major challenge for imaging at highest contrasts is the minimization of quasi-static PSF residuals left over by the FPWS and the coronagraph. In order to reach the EPICS contrast requirements of $10^{-9}$ and assuming a speckle calibration efficiency by data reduction of about $10^{-3}$ (reasonable assumption since on the one hand the simulated efficiency is somewhat better and there's an additional gain provided by ADI, but on the other hand the required PSF residuals should be 5 times lower to achieve the contrast at SNR of 5), quasi-static PSF residuals should be of the order $10^{-6}$ of the image peak intensity. Considering that each second order speckle corresponds to one Fourier components of the WFE, the Maréchal equation provides us with a residual WFE requirement per Fourier component of about 0.3 nm rms. Since the EPICS FoV of about one square-arcsecond may contain up to 16000 speckles (speckle FWHM ~8mas in H-band for a 42-m aperture), the required residual WFE would be around 0.3×sqrt(16000) = 40 nm rms for equally distributed aberrations.

Although certainly very challenging, even higher levels of quasi-static aberration compensation have already been achieved in the laboratory[5]. Figure 12 and Figure 13 show the capability of the DM to correct for aberrations inside its spatial control bandwidth. Typically, instrumental speckles can be reduced by factors of at least $10^4$ largely increasing the error budget for quasi-static aberration to a few tens of nm rms per Fourier component. Figure 13 further shows that fitting real influence functions (of the BMM MEMS DM in this case), creates a small residual WFE at higher spatial frequencies which however hardly impacts on the achievable contrast in the central region of interest.

A somewhat special case are the phasing errors introduced by the segmented primary mirror of the telescope. A similar study as the one displayed in Figure 13 has been performed replacing the sine aberration by a step function. In this case, the DM is less efficient in fitting the aberration and the residual speckle intensity is reduced by no more than $10^2$-$10^3$ of

the original intensity. Yaitskova (this conference) studied the effect of telescope segment aberrations analytically and independently find a level of about 80 nm rms required to reach a contrast level $10^{-6}$ with the XAO.

Coronagraph residuals generally need to be at about the same level as residual speckles, but it must be considered that interference between the two (pinned speckles) may somewhat increase the intensity with respect to the sum of the individual terms. A coronagraphic efficiency of $5\times10^{-6}$ at $5\lambda/D$ has already been demonstrated with the EPICS baseline coronagraph (see Figure 7).

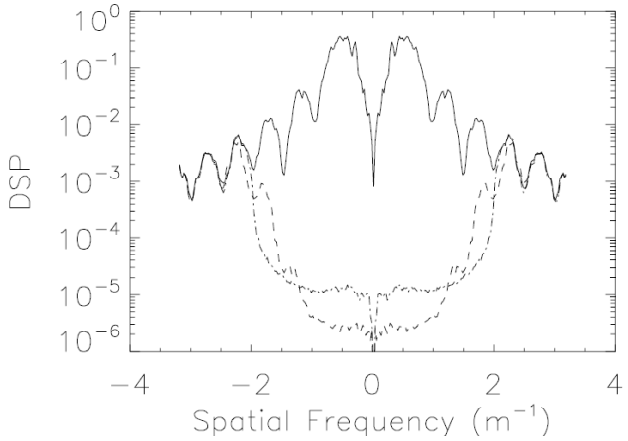


**Figure 12. PSF profiles before and after correction by a DM. Solid: uncorrected coronagraphic PSF profile (or aberration PSD). Dashed: Profile obtained after least-squares correction by a DM. Dashed-dotted: Profile obtained with Fourier filtering used for initial analysis of EPICS (from Verinaud et al. this conference).**

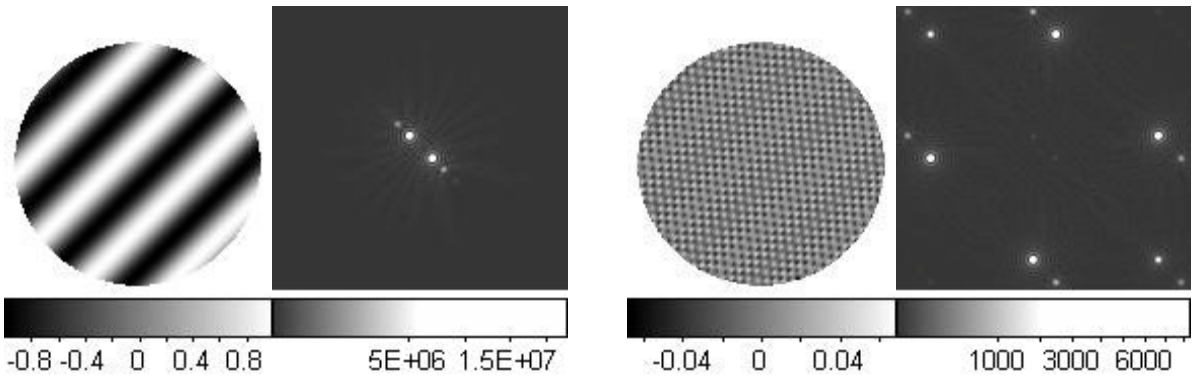


**Figure 13. Capability of the BMM to correct for a sinusoidal aberration. Left: Input aberration WFE and corresponding image obtained with a perfect coronagraph. Right: Residual WFE and corresponding coronagraphic image after correction by the BMM. The inner correction area of the DM is clean and the speckles in the central area are reduced by over a factor better than $10^4$.**

### 3.4 Differential aberrations

Strictly differential data reduction techniques are foreseen for the IFS innermost FoV (inside the bifurcation point) and for E-POL. For these techniques, differential aberrations in the distinct detection channels must be extremely small since they are not corrected by the XAO, and there is no additional data reduction step (apart from ADI which we ignore for now) that mitigates their impact. Differential speckles connect to features of the residual coronagraphic PSF and are proportional to those in intensity. Since the dominant such feature is usually the coronagraphic PSF core (typical level $10^{-3}$ compared to $10^{-5}$ – $10^{-6}$ for the quasi-static residuals discussed in the previous section), differential speckles must be at a level of $10^{-6}$ (or around 0.3 nm rms per Fourier component) to reach the required $10^{-9}$ contrast.

In contrast to the quasi-static aberrations discussed in the previous section, this optical quality requirement must not rely on correction by an active component and has to be guaranteed by design. A lenslet-based IFS, however, not contain differential optical elements since the FoV is chopped up by the lenslet aray located in front of the dispersing element. For E-POL, the only optical component that strictly introduces differential aberrations is the FLC for which extremely low values of about 1 nm rms have been measured (see Figure 9, right), and a prototype with hopefully even better optical goal quality of 0.5 nm rms total phase differential wave front error has been ordered and will be evaluated during EPICS phase-A.

## 4. CONCLUSIONS

Phase 1 of the EPICS phase-A study consisting of end-to-end modeling, trade-off studies and conceptual design will end with the phase 1 review end of September 2008. So far, the initial study results did not identify show-stoppers preventing EPICS from reaching its science goals. All potentially important contributors to the error budget such as gaps between the segments of the telescope primary mirror, amplitude errors due to reflectivity variations between segments, chromatic beamshift on the optics in front of the ADC due to atmospheric refraction, light scattering related to cleanliness of optics, ghosts, and Fresnel propagation of out-of-pupil aberrations will be analyzed and specified during phase 1.

Apart from instrument concept and development plan, a precise error budget including a long list of contributors will be available and some key enabling technologies will have been prototyped by the end of the phase-A study in 2010. These results in combination with the invaluable experience that will be obtained from upcoming instruments such as SPHERE (Beuzit et al., this conference) and GPI (Macintosh et al., this conference) will set the path for Exoplanet science with extremely larger ground-based telescopes.

## REFERENCES


[1] Antichi, A. et al., submitted to ApJ, 2008
[2] Butler, R.P. et al. ApJ 646, 505-, 2006
[3] Cavarroc, C.; Boccaletti, A.; Baudoz, P.; Fusco, T.; Rouan, D, A&A 447, pp.397-, 2006
[4] Conan, R.; Hampton, P.; Bradley, C.; Keskin, O., Proc SPIE, Vol 6272, pp. 62721V, 2006
[5] Evans, J. W. et al., Optics Express, vol. 14, Issue 12, pp.5558-5570, 2006
[6] Liou et al., AJ 118, pp. 580-590, 1999
[7] Macintosh, B.; Poyneer, L.; Sivaramakrishnan, A.; Marois, C. Proc SPIE, Vol 5903, pp. 170-177, 2005
[8] Marois, C., Doyon, R., Racine, R., Nadeau, D., PASP, 112, 91, 2000
[9] Marois, C.; Lafrenière, D.; Doyon, R.; Macintosh, B.; Nadeau, D., AJ 641, Issue 1, pp. 556-564, 2006
[10] Mordasini, C., Alibert, Y., Benz, W. et al., arXiv0710.5667, 2007
[11] Moro-Martin & Malhotra, AJ 124, Issue 4, pp. 2305-2321, 2002
[12] Poyneer, L. A.; Macintosh, B., JOSA A, vol. 21, Issue 5, pp.810-81, 2004
[13] Sparks, W.B.; Ford H.C., ApJ 578:543–564, 2002
[14] Thatte, N., Abuter, R., Tecza, M., Nielsen, E.L., Clarke, F.J., Close, L.M., MNRAS, 378, 1229, 2007
[15] Vérinaud, C.; Le Louarn, M.; Korkiakoski, V.; Carbillet, M, MNRAS 357L, Issue 1, pp. L26-L30, 2005
[16] Schmid et al., in: ``Direct imaging of Exoplanets'', IAU Coll. 200, p. 165, 2006
[17] Stam, D. et al., A&A 482, 989, 2008